Search for high mass $\gamma\gamma$ resonances in e$^+$e$^-$ $\rightarrow \ell^+\ell^-\gamma\gamma$, $\nu\overline{\nu}\gamma\gamma$ and q$\overline{\text{q}}\gamma\gamma$ at LEP I

DELPHI Collaboration

P.Abreu[21], W.Adam[50], T.Adye[37], E.Agasi[31], I.Ajinenko[42], R.Aleksan[39], G.D.Alekseev[16], R.Alemany[49], P.P.Allport[22], S.Almehed[24], U.Amaldi[9], S.Amato[47], A.Andreazza[28], M.L.Andrieux[14], P.Antilogus[9], W-D.Apel[17], Y.Arnoud[39], B.Åsman[44], J-E.Augustin[25], A.Augustinus[9], P.Baillon[9], P.Bambade[19], F.Barao[21], R.Barate[14], M.Barbi[47], D.Y.Bardin[16], A.Baroncelli[40], O.Barring[24], J.A.Barrio[26], W.Bartl[50], M.J.Bates[37], M.Battaglia[15], M.Baubillier[23], J.Baudot[39], K-H.Becks[52], M.Begalli[6], P.Beilliere[8], Yu.Belokopytov[9,53], A.C.Benvenuti[5], M.Berggren[47], D.Bertini[25], D.Bertrand[2], F.Bianchi[45], M.Bigi[45], M.S.Bilenky[16], P.Billoir[23], D.Bloch[10], M.Blume[52], T.Bolognese[39], M.Bonesini[28], W.Bonivento[28], P.S.L.Booth[22], G.Borisov[42], C.Bosio[40], O.Botner[48], E.Boudinov[31], B.Bouquet[19], C.Bourdarios[9], T.J.V.Bowcock[22], M.Bozzo[13], P.Branchini[40], K.D.Brand[36], T.Brenke[52], R.A.Brenner[15], C.Bricman[2], R.C.A.Brown[9], P.Bruckman[18], J-M.Brunet[8], L.Bugge[33], T.Buran[33], T.Burgsmueller[52], P.Buschmann[52], A.Buys[9], S.Cabrera[49], M.Caccia[28], M.Calvi[28], A.J.Camacho Rozas[41], T.Camporesi[9], V.Canale[38], M.Canepa[13], K.Cankocak[44], F.Cao[2], F.Carena[9], L.Carroll[22], C.Caso[13], M.V.Castillo Gimenez[49], A.Cattai[9], F.R.Cavallo[5], V.Chabaud[9], Ph.Charpentier[9], L.Chaussard[25], P.Checchia[36], G.A.Chelkov[16], M.Chen[2], R.Chierici[45], P.Chliapnikov[42], P.Chochula[7], V.Chorowicz[9], J.Chudoba[30], V.Cindro[43], P.Collins[9], J.L.Contreras[19], R.Contri[13], E.Cortina[49], G.Cosme[19], F.Cossutti[46], H.B.Crawley[1], D.Crennell[37], G.Crosetti[13], J.Cuevas Maestro[34], S.Czellar[15], E.Dahl-Jensen[29], J.Dahm[52], B.Dalmagne[19], M.Dam[29], G.Damgaard[29], P.D.Dauncey[37], W.Davenport[9], W.Da Silva[23], C.Defoix[8], A.Deghorain[2], G.Della Ricca[46], P.Delpierre[27], N.Demaria[35], A.De Angelis[9], W.De Boer[17], S.De Brabandere[2], C.De Clercq[2], C.De La Vaissiere[23], B.De Lotto[46], A.De Min[36], L.De Paula[47], C.De Saint-Jean[39], H.Dijkstra[9], L.Di Ciaccio[38], F.Djama[10], J.Dolbeau[8], M.Donszelmann[9], K.Doroba[51], M.Dracos[10], J.Drees[52], K.-A.Drees[52], M.Dris[32], J-D.Durand[25], D.Edsall[1], R.Ehret[17], G.Eigen[4], T.Ekelof[48], G.Ekspong[44], M.Elsing[52], J-P.Engel[10], B.Erzen[43], M.Espirito Santo[21], E.Falk[24], D.Fassouliotis[32], M.Feindt[9], A.Fenyuk[42], A.Ferrer[49], S.Fichet[23], T.A.Filippas[32], A.Firestone[1], P.-A.Fischer[10], H.Foeth[9], E.Fokitis[32], F.Fontanelli[13], F.Formenti[9], B.Franek[37], P.Frenkiel[8], D.C.Fries[17], A.G.Frodesen[4], R.Fruhwirth[50], F.Fulda-Quenzer[19], J.Fuster[49], A.Galloni[22], D.Gamba[45], M.Gandelman[6], C.Garcia[49], J.Garcia[41], C.Gaspar[9], U.Gasparini[36], Ph.Gavillet[9], E.N.Gazis[32], D.Gele[10], J-P.Gerber[10], M.Gibbs[22], R.Gokieli[51], B.Golob[43], G.Gopal[37], L.Gorn[1], M.Gorski[51], Yu.Gouz[45,53], V.Gracco[13], E.Graziani[40], G.Grosdidier[19], K.Grzelak[51], S.Gumenyuk[28,53], P.Gunnarsson[44], M.Gunther[48], J.Guy[37], F.Hahn[9], S.Hahn[52], A.Hallgren[48], K.Hamacher[52], W.Hao[31], F.J.Harris[35], V.Hedberg[24], R.Henriques[21], J.J.Hernandez[49], P.Herquet[2], H.Herr[9], T.L.Hessing[35], E.Higon[49], H.J.Hilke[9], T.S.Hill[1], S-O.Holmgren[44], P.J.Holt[35], D.Holthuizen[31], S.Hoorelbeke[2], M.Houlden[22], J.Hrubec[50], K.Huet[2], K.Hultqvist[44], J.N.Jackson[22], R.Jacobsson[44], P.Jalocha[18], R.Janik[7], Ch.Jarlskog[24], G.Jarlskog[24], P.Jarry[39], B.Jean-Marie[19], E.K.Johansson[44], L.Jonsson[24], P.Jonsson[24], C.Joram[9], P.Juillot[10], M.Kaiser[17], F.Kapusta[23], K.Karafasoulis[11], M.Karlsson[44], E.Karvelas[11], S.Katsanevas[3], E.C.Katsoufis[32], R.Keranen[4], Yu.Khokhlov[42], B.A.Khomenko[16], N.N.Khovanski[16], B.King[22], N.J.Kjaer[29], H.Klein[9], A.Klovning[4], P.Kluit[31], B.Koene[31], P.Kokkinias[11], M.Koratzinos[9], K.Korcyl[18], C.Kourkoumelis[3], O.Kouznetsov[13,16], P.-H.Kramer[52], M.Krammer[50], C.Kreuter[17], I.Kronkvist[24], Z.Krumstein[16], W.Krupinski[18], P.Kubinec[7], W.Kucewicz[18], K.Kurvinen[15], C.Lacasta[49], I.Laktineh[25], J.W.Lamsa[1], L.Lanceri[46], D.W.Lane[1], P.Langefeld[52], I.Last[22], J-P.Laugier[39], R.Lauhakangas[15], G.Leder[50], F.Ledroit[14], V.Lefebure[2], C.K.Legan[1], R.Leitner[30], Y.Lemoigne[39], J.Lemonne[2], G.Lenzen[52], V.Lepeltier[19], T.Lesiak[18], J.Libby[35], D.Liko[50], R.Lindner[52], A.Lipniacka[36], I.Lippi[36], B.Loerstad[24], J.G.Loken[35], J.M.Lopez[41], D.Loukas[11], P.Lutz[39], L.Lyons[35], J.MacNaughton[50], G.Maehlum[17], A.Maio[21], T.G.M.Malmgren[44], V.Malychev[16], F.Mandl[50], J.Marco[41], R.Marco[41], B.Marechal[47], M.Margoni[36], J-C.Marin[9], C.Mariotti[40], A.Markou[11], T.Maron[52], C.Martinez-Rivero[41], F.Martinez-Vidal[49], S.Marti i Garcia[49], J.Masik[30], F.Matorras[41], C.Matteuzzi[9], G.Matthiae[38], M.Mazzucato[36], M.Mc Cubbin[9], R.Mc Kay[1], R.Mc Nulty[22], J.Medbo[48], M.Merk[31], C.Meroni[28], S.Meyer[17], W.T.Meyer[1], A.Miagkov[42], M.Michelotto[36], E.Migliore[45], L.Mirabito[25], W.A.Mitaroff[50], U.Mjoernmark[24], T.Moa[44], R.Moeller[29], K.Moenig[9], M.R.Monge[13], P.Morettini[13], H.Mueller[17], L.M.Mundim[6], W.J.Murray[37], B.Muryn[18], G.Myatt[35], F.Naraghi[14], F.L.Navarria[5], S.Navas[49], K.Nawrocki[51], P.Negri[28], W.Neumann[52], N.Neumeister[50], R.Nicolaidou[3], B.S.Nielsen[29], M.Nieuwenhuizen[31], V.Nikolaenko[10], P.Niss[44], A.Nomerotski[36], A.Normand[35], M.Novak[12], W.Oberschulte-Beckmann[17], V.Obraztsov[42], A.G.Olshevski[16], A.Onofre[21], R.Orava[15], K.Osterberg[15], A.Ouraou[39], P.Paganini[19], M.Paganoni[9], P.Pages[10], R.Pain[23], H.Palka[18], Th.D.Papadopoulou[32], K.Papageorgiou[11], L.Pape[9], C.Parkes[35], F.Parodi[13], A.Passeri[40], M.Pegoraro[36], L.Peralta[21], M.Pernicka[50], A.Perrotta[5], C.Petridou[46], A.Petrolini[13], M.Petrovyck[28,53], H.T.Phillips[37], G.Piana[13], F.Pierre[39], M.Pimenta[21], S.Plaszczynski[19], O.Podobrin[17], M.E.Pol[6], G.Polok[18], P.Poropat[46], V.Pozdniakov[16], M.Prest[46], P.Privitera[38], N.Pukhaeva[16], A.Pullia[28], D.Radojicic[35], S.Ragazzi[28], H.Rahmani[32], P.N.Ratoff[20], A.L.Read[33], M.Reale[52], P.Rebecchi[19], N.G.Redaelli[28], M.Regler[50], D.Reid[9], P.B.Renton[35], L.K.Resvanis[3], F.Richard[19], J.Richardson[22], J.Ridky[12], G.Rinaudo[45],

I.Ripp[39], A.Romero[45], I.Roncagliolo[13], P.Ronchese[36], L.Roos[14], E.I.Rosenberg[1], E.Rosso[9], P.Roudeau[19], T.Rovelli[5], W.Ruckstuhl[31], V.Ruhlmann-Kleider[39], A.Ruiz[41], H.Saarikko[15], Y.Sacquin[39], A.Sadovsky[16], O.Sahr[14], G.Sajot[14], J.Salt[49], J.Sanchez[26], M.Sannino[13], M.Schimmelpfennig[17], H.Schneider[17], U.Schwickerath[17], M.A.E.Schyns[52], G.Sciolla[45], F.Scuri[46], P.Seager[20], Y.Sedykh[16], A.M.Segar[35], A.Seitz[17], R.Sekulin[37], L.Serbelloni[38], R.C.Shellard[6], I.Siccama[31], P.Siegrist[39], S.Simonetti[39], F.Simonetto[36], A.N.Sisakian[16], B.Sitar[7], T.B.Skaali[33], G.Smadja[25], N.Smirnov[42], O.Smirnova[24], G.R.Smith[37], O.Solovianov[42], R.Sosnowski[51], D.Souza-Santos[6], T.Spassov[21], E.Spiriti[40], P.Sponholz[52], S.Squarcia[13], C.Stanescu[40], S.Stapnes[33], I.Stavitski[36], K.Stevenson[35], F.Stichelbaut[9], A.Stocchi[19], J.Strauss[50], R.Strub[10], B.Stugu[4], M.Szczekowski[51], M.Szeptycka[51], T.Tabarelli[28], J.P.Tavernet[23], O.Tchikilev[42], J.Thomas[35], A.Tilquin[27], J.Timmermans[31], L.G.Tkatchev[16], T.Todorov[10], S.Todorova[10], D.Z.Toet[31], A.Tomaradze[2], A.Tonazzo[28], L.Tortora[40], G.Transtromer[24], D.Treille[9], W.Trischuk[9], G.Tristram[8], A.Trombini[19], C.Troncon[28], A.Tsirou[9], M-L.Turluer[39], I.A.Tyapkin[16], M.Tyndel[37], S.Tzamarias[22], B.Ueberschaer[52], O.Ullaland[9], V.Uvarov[42], G.Valenti[5], E.Vallazza[9], C.Vander Velde[2], G.W.Van Apeldoorn[31], P.Van Dam[31], J.Van Eldik[31], N.Vassilopoulos[35], G.Vegni[28], L.Ventura[36], W.Venus[37], F.Verbeure[2], M.Verlato[36], L.S.Vertogradov[16], D.Vilanova[39], P.Vincent[25], L.Vitale[46], E.Vlasov[42], A.S.Vodopyanov[16], V.Vrba[12], H.Wahlen[52], C.Walck[44], F.Waldner[46], M.Weierstall[52], P.Weilhammer[9], C.Weiser[17], A.M.Wetherell[9], D.Wicke[52], J.H.Wickens[2], M.Wielers[17], G.R.Wilkinson[35], W.S.C.Williams[35], M.Winter[10], M.Witek[18], K.Woschnagg[48], K.Yip[35], O.Yushchenko[42], F.Zach[25], A.Zaitsev[42], A.Zalewska[9], P.Zalewski[51], D.Zavrtanik[43], E.Zevgolatakos[11], N.I.Zimin[16], M.Zito[39], D.Zontar[43], G.C.Zucchelli[44], G.Zumerle[36]

[1] Ames Laboratory and Department of Physics, Iowa State University, Ames IA 50011, USA
[2] Physics Department, Univ. Instelling Antwerpen, Universiteitsplein 1, B-2610 Wilrijk, Belgium
 and IIHE, ULB-VUB, Pleinlaan 2, B-1050 Brussels, Belgium
 and Faculté des Sciences, Univ. de l'Etat Mons, Av. Maistriau 19, B-7000 Mons, Belgium
[3] Physics Laboratory, University of Athens, Solonos Str. 104, GR-10680 Athens, Greece
[4] Department of Physics, University of Bergen, Allégaten 55, N-5007 Bergen, Norway
[5] Dipartimento di Fisica, Università di Bologna and INFN, Via Irnerio 46, I-40126 Bologna, Italy
[6] Centro Brasileiro de Pesquisas Físicas, rua Xavier Sigaud 150, RJ-22290 Rio de Janeiro, Brazil
 and Depto. de Física, Pont. Univ. Católica, C.P. 38071 RJ-22453 Rio de Janeiro, Brazil
 and Inst. de Física, Univ. Estadual do Rio de Janeiro, rua São Francisco Xavier 524, Rio de Janeiro, Brazil
[7] Comenius University, Faculty of Mathematics and Physics, Mlynska Dolina, SK-84215 Bratislava, Slovakia
[8] Collège de France, Lab. de Physique Corpusculaire, IN2P3-CNRS, F-75231 Paris Cedex 05, France
[9] CERN, CH-1211 Geneva 23, Switzerland
[10] Centre de Recherche Nucléaire, IN2P3 - CNRS/ULP - BP20, F-67037 Strasbourg Cedex, France
[11] Institute of Nuclear Physics, N.C.S.R. Demokritos, P.O. Box 60228, GR-15310 Athens, Greece
[12] FZU, Inst. of Physics of the C.A.S. High Energy Physics Division, Na Slovance 2, 180 40, Praha 8, Czech Republic
[13] Dipartimento di Fisica, Università di Genova and INFN, Via Dodecaneso 33, I-16146 Genova, Italy
[14] Institut des Sciences Nucléaires, IN2P3-CNRS, Université de Grenoble 1, F-38026 Grenoble Cedex, France
[15] Research Institute for High Energy Physics, SEFT, P.O. Box 9, FIN-00014 Helsinki, Finland
[16] Joint Institute for Nuclear Research, Dubna, Head Post Office, P.O. Box 79, 101 000 Moscow, Russian Federation
[17] Institut für Experimentelle Kernphysik, Universität Karlsruhe, Postfach 6980, D-76128 Karlsruhe, Germany
[18] Institute of Nuclear Physics and University of Mining and Metalurgy, Ul. Kawiory 26a, PL-30055 Krakow, Poland
[19] Université de Paris-Sud, Lab. de l'Accélérateur Linéaire, IN2P3-CNRS, Bât. 200, F-91405 Orsay Cedex, France
[20] School of Physics and Chemistry, University of Lancaster, Lancaster LA1 4YB, UK
[21] LIP, IST, FCUL - Av. Elias Garcia, 14-1°, P-1000 Lisboa Codex, Portugal
[22] Department of Physics, University of Liverpool, P.O. Box 147, Liverpool L69 3BX, UK
[23] LPNHE, IN2P3-CNRS, Universités Paris VI et VII, Tour 33 (RdC), 4 place Jussieu, F-75252 Paris Cedex 05, France
[24] Department of Physics, University of Lund, Sölvegatan 14, S-22363 Lund, Sweden
[25] Université Claude Bernard de Lyon, IPNL, IN2P3-CNRS, F-69622 Villeurbanne Cedex, France
[26] Universidad Complutense, Avda. Complutense s/n, E-28040 Madrid, Spain
[27] Univ. d'Aix - Marseille II - CPP, IN2P3-CNRS, F-13288 Marseille Cedex 09, France
[28] Dipartimento di Fisica, Università di Milano and INFN, Via Celoria 16, I-20133 Milan, Italy
[29] Niels Bohr Institute, Blegdamsvej 17, DK-2100 Copenhagen 0, Denmark
[30] NC, Nuclear Centre of MFF, Charles University, Areal MFF, V Holesovickach 2, 180 00, Praha 8, Czech Republic
[31] NIKHEF-H, Postbus 41882, NL-1009 DB Amsterdam, The Netherlands
[32] National Technical University, Physics Department, Zografou Campus, GR-15773 Athens, Greece
[33] Physics Department, University of Oslo, Blindern, N-1000 Oslo 3, Norway
[34] Dpto. Fisica, Univ. Oviedo, C/P. Pérez Casas, S/N-33006 Oviedo, Spain
[35] Department of Physics, University of Oxford, Keble Road, Oxford OX1 3RH, UK
[36] Dipartimento di Fisica, Università di Padova and INFN, Via Marzolo 8, I-35131 Padua, Italy
[37] Rutherford Appleton Laboratory, Chilton, Didcot OX11 OQX, UK
[38] Dipartimento di Fisica, Università di Roma II and INFN, Tor Vergata, I-00173 Rome, Italy
[39] CEA, DAPNIA/Service de Physique des Particules, CE-Saclay, F-91191 Gif-sur-Yvette Cedex, France
[40] Istituto Superiore di Sanità, Ist. Naz. di Fisica Nucl. (INFN), Viale Regina Elena 299, I-00161 Rome, Italy
[41] Instituto de Fisica de Cantabria (CSIC-UC), Avda. los Castros, S/N-39006 Santander, Spain, (CICYT-AEN93-0832)
[42] Inst. for High Energy Physics, Serpukov P.O. Box 35, Protvino, (Moscow Region), Russian Federation
[43] J. Stefan Institute and Department of Physics, University of Ljubljana, Jamova 39, SI-61000 Ljubljana, Slovenia
[44] Fysikum, Stockholm University, Box 6730, S-113 85 Stockholm, Sweden
[45] Dipartimento di Fisica Sperimentale, Università di Torino and INFN, Via P. Giuria 1, I-10125 Turin, Italy
[46] Dipartimento di Fisica, Università di Trieste and INFN, Via A. Valerio 2, I-34127 Trieste, Italy
 and Istituto di Fisica, Università di Udine, I-33100 Udine, Italy

[47] Univ. Federal do Rio de Janeiro, C.P. 68528 Cidade Univ., Ilha do Fundão BR-21945-970 Rio de Janeiro, Brazil
[48] Department of Radiation Sciences, University of Uppsala, P.O. Box 535, S-751 21 Uppsala, Sweden
[49] IFIC, Valencia-CSIC, and D.F.A.M.N., U. de Valencia, Avda. Dr. Moliner 50, E-46100 Burjassot (Valencia), Spain
[50] Institut für Hochenergiephysik, Österr. Akad. d. Wissensch., Nikolsdorfergasse 18, A-1050 Vienna, Austria
[51] Inst. Nuclear Studies and University of Warsaw, Ul. Hoza 69, PL-00681 Warsaw, Poland
[52] Fachbereich Physik, University of Wuppertal, Postfach 100 127, D-42097 Wuppertal, Germany
[53] On leave of absence from IHEP Serpukhov

Abstract. A search for high mass photon pairs from the processes $e^+e^- \rightarrow \ell^+\ell^-\gamma\gamma$, $e^+e^- \rightarrow q\bar{q}\gamma\gamma$ and $e^+e^- \rightarrow \nu\bar{\nu}\gamma\gamma$ with the DELPHI detector at LEP I is reported. From a data sample containing 3.5 million hadronic Z^0 decays, collected by DELPHI during the years 1991 to 1994, 79 events with two charged leptons and two isolated photons were selected with photon pair masses above 10 GeV/c^2, where 76 ± 6 events were predicted from standard sources. In the same data sample, no $\nu\bar{\nu}\gamma\gamma$ candidates were found and no accumulation of events was visible for $\gamma\gamma$ masses above 10 GeV/c^2 in the q$\bar{q}\gamma\gamma$ channel. Upper limits at 95% confidence level on the Z^0 branching ratios for the three different channels were extracted from the data. In the mass region $m_{\gamma\gamma} > 30$ GeV/c^2 the limits obtained are between 3×10^{-6} and 4×10^{-6}.

1 Introduction

The search for a high mass resonance decaying into $\gamma\gamma$ is motivated by a study of $\ell^+\ell^-\gamma\gamma$ events by the L3 Collaboration [1]. They reported the observation of events with photon-photon masses of about 60 GeV/c^2 which suggested the production of a new particle. The other LEP collaborations, OPAL [2] and ALEPH [3], extended this search to include two other potential decay channels, $\nu\bar{\nu}\gamma\gamma$ and q$\bar{q}\gamma\gamma$. In addition new theoretical models were proposed to explain these events [4].

The search reported below used a sample of events corresponding to a luminosity of about 110 pb^{-1} collected by the DELPHI experiment at LEP from 1991 to 1994, looking for evidence of a heavy resonance decaying to $\gamma\gamma$ in the $\ell^+\ell^-\gamma\gamma$, $\nu\bar{\nu}\gamma\gamma$ and q$\bar{q}\gamma\gamma$ channels.

2 Apparatus

A detailed description of the DELPHI apparatus can be found in [5]. For the present analysis the following parts of the detector were most relevant:

- for the measurement of charged particles the Microvertex Detector (VD), the Inner Detector (ID), the Time Projection Chamber (TPC), the Outer Detector (OD) and the Forward Chambers A and B (FCA, FCB);
- the Small Angle Tagger (SAT) and the Small angle TIle Calorimeter (STIC), which were the main luminosity monitors (the SAT operated until 1993, and STIC in 1994), were also used to detect electromagnetic showers at very low polar angle;

- for the trigger, besides the detectors mentioned above, the barrel Time-Of-Flight counters (TOF), the endcap scintillators (HOF) and a scintillator layer embedded in the barrel electromagnetic calorimeter (HPC);
- for the measurement of the electromagnetic energy the High-density Projection Chamber (HPC) and the Forward Electromagnetic Calorimeter (FEMC);
- for the measurement of the hadronic energy and muon identification the Hadron Calorimeter (HCAL), which covers both the barrel and endcap regions;
- for muon identification the barrel (MUB) and endcap (MUF) muon chambers.

The ID and TPC cover the angular range $20° < \theta < 160°$ (throughout this paper, θ is the polar angle defined with respect to the beam axis and ϕ is the azimuthal angle), the OD covers the range $43° < \theta < 137°$ and the FCA/FCB cover the range $11° < \theta < 33°$ and $147° < \theta < 169°$. Within the barrel region, defined as the angular acceptance of the OD, the momentum measurement precision for 45 GeV/c muons is $\sigma(p)/p^2 = 0.6\times10^{-3}$ (GeV/c)$^{-1}$, using the combined information from the detectors VD+ID+TPC+OD. In the endcap region the resolution degrades, and for 45 GeV/c muons is $\sigma(p)/p^2 = 1.5 \times 10^{-3}$ (GeV/c)$^{-1}$ for polar angles between $25°$ and $30°$. The MUB covers the interval $52° < \theta < 128°$ whilst the MUF extends over the range $9° < \theta < 43°$ and $137° < \theta < 171°$.

The HPC has the same angular coverage as the OD, whilst the FEMC covers an interval slightly larger than the FCA/FCB. The HCAL covers the entire barrel and endcap regions over the range $10° < \theta < 170°$. The SAT and the STIC cover the regions $2.3° < \theta < 7.7°$ and $1.7° < \theta < 10.9°$, respectively. The energy resolution of the electromagnetic calorimeter is $\sigma(E)/E = \sqrt{(0.043)^2 + (0.32/\sqrt{E})^2}$ (E in GeV) in the barrel region and $\sigma(E)/E = \sqrt{(0.03)^2 + (0.12/\sqrt{E})^2 + (0.11/E)^2}$ (E in GeV) in the forward region. The HCAL energy resolution is $\sigma(E)/E = \sqrt{(0.21)^2 + (1.12/\sqrt{E})^2}$ (E in GeV).

For the topologies selected in this analysis, the trigger efficiency was close to 1 for all channels. Unless otherwise stated the value taken for this efficiency was 100%.

3 Decays into two charged leptons and two photons

The search for events with two isolated photons and a charged lepton pair relied on topological criteria to select leptonic events with two isolated photons. The three leptonic channels were afterwards classified as $e^+e^-\gamma\gamma$, $\mu^+\mu^-\gamma\gamma$ and
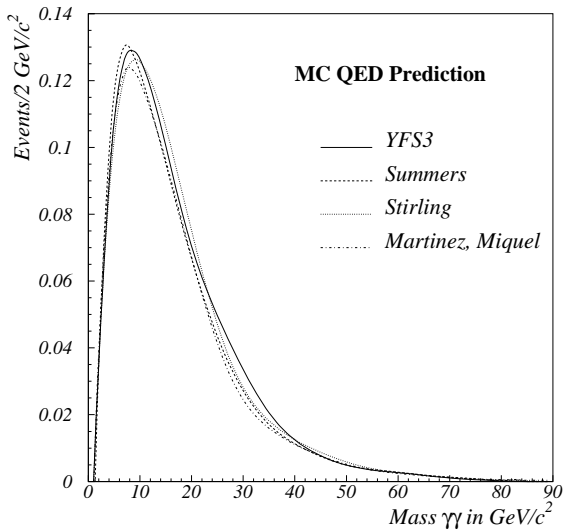
Fig. 1. Comparison of the $\gamma\gamma$ mass distribution for doubly radiative leptonic events from the different Monte Carlo generators. The curves were normalized to the same number of events

$\tau^+\tau^-\gamma\gamma$, according to criteria based on the comparison between the measured momenta and the four particles in the event and the momenta calculated from their angles (see Sect. 3.2).

The observed distributions of $\ell^+\ell^-\gamma\gamma$ events, obtained after the selections, were compared with second order QED predictions, obtained through Monte Carlo simulations. Details of the generators used, the analysis and the results are reported in Sects. 3.1, 3.2 and 3.3 respectively.

3.1 Monte Carlo generators

There are several generators generally available, which make use of higher order QED corrections in order to simulate doubly radiative leptonic events. Stirling's generator [6] includes only the largest source of this type of event: final state radiation (FSR). The generator from Jadach and Ward (YFS3) [7] includes both hard FSR and initial state radiation (ISR) calculated in the next-to-leading-log approximation. It also uses exponentiation to take into account the contribution from soft photons, thereby providing the correct absolute value for the total cross-section. Summer's program [8] includes exact second order ISR and FSR, mass effects, and both γ and Z^0 exchange. Finally, the generator from Martinez and Miquel [9] includes the same contributions as Summer's program and, in addition, the t -channel contribution for the e^+e^- process.

A comparison between the predictions of these four generators is found in Fig. 1, where the photon-photon mass spectrum is presented for the events passing topological selection criteria similar to those described in Sect. 3.2. The predicted spectra are in agreement.

The YFS3 Monte Carlo generator was used to generate the events for the three channels. The tracking of the different particles and the response of the DELPHI detector was afterwards simulated using the DELPHI package, DELSIM [5].

Events of the type $e^+e^- \rightarrow Z^0 \rightarrow \ell^+\ell^-X$, $X \rightarrow \gamma\gamma$, with X having a mass of 10 GeV/c^2 and 60 GeV/c^2 were generated for the three lepton channels using the PYTHIA package [10]. The X particle was generated according to the Bjorken process for the production of the standard Higgs boson. These events were used to check the selection criteria and efficiencies.

3.2 Data analysis

The analysis was based on the topology of the events, to select $\ell^+\ell^-\gamma\gamma$ channels, and on the difference between the measured momenta of the particles and the momenta calculated from the measured angles and the condition of energy and momentum conservation, which enabled the identification of the different lepton channels under study.

The events were selected according to the following criteria:

- They should contain between two and six charged particles, of which at least two are not photon conversions before or at the TPC inner wall, and have a momentum greater than 1 GeV/c , a polar angle between $20°$ and $160°$, and impact parameters in the transverse plane and in the beam direction below 5 cm and 10 cm respectively. The tracks of these two particles must also be isolated from each other by at least $20°$. Events with charge multiplicities up to six were retained at this level, because of the possible decay products of τ leptons in the $\tau^+\tau^-\gamma\gamma$ channel. In these events, the two most energetic charged particles satisfying these criteria were the ones considered in the subsequent analysis. Pairs of oppositely charged particles were considered as resulting from photon conversion if their invariant mass was less than 80 MeV/c^2 and the closest distance of approach between their trajectories in the transverse plane was lower than 4.5 cm.
- The events should contain at least two photons isolated from the nearest charged particle and from each other by at least $15°$. The two most energetic photons satisfying this criterion were required in addition to have an energy of at least 3 GeV and polar angle between $20°$ and $160°$. These were the two photons considered in the subsequent analysis. These cuts reject the majority of radiative photons, and photons from π^0 in τ decays.
- There should be no more than one converted photon.

The momenta of the particles were calculated for the events satisfying the above selection criteria imposing, in addition, the requirements of energy and momentum conservation. This calculation relied on the good measurement of the angles. In the $\tau^+\tau^-\gamma\gamma$ channel, most of the final charged particles resulting from the τ decays follow the τ direction.

For $\gamma\gamma$ masses around 60 GeV/c^2, the calculation improved the mass resolution in the $e^+e^-\gamma\gamma$ and $\mu^+\mu^-\gamma\gamma$ channels by a factor of about three to about 1 GeV/c^2.

The effect of undetected photons inside the beam pipe due to initial state radiation was studied through Monte Carlo simulation. The magnitude of this loss is usually small ($<$

2 GeV). Its contribution to the mass resolution was estimated for events with photon-photon masses greater than 50 GeV/c^2 and is shown later.

Independent comparisons between measured and calculated momenta were made for charged particles and for photons. While in e$^+$e$^-\gamma\gamma$ and $\mu^+\mu^-\gamma\gamma$ channels calculated and measured momenta should agree for both photons and charged particles, in the $\tau^+\tau^-\gamma\gamma$ channel differences are expected due to the neutrino emission, especially for the charged particles. The comparisons were based on χ^2. For charged particles, the χ^2 was defined by:

$$\chi^2_{charged} = \sum_{i=1,2} \left(\frac{p_{i_{measured}} - p_{i_{calc}}}{\sigma(p_i)} \right)^2$$

where $p_{measured}$ and p_{calc} are the measured momentum and the momentum obtained from the calculation, respectively. For electrons, either the momentum or the calorimetric electromagnetic energy was used for $p_{measured}$, depending on which gave rise to the lowest $\chi^2_{charged}$ value. For photons, $\chi^2_{photons}$ was defined the same way with $p_{measured}=E_{measured}$ and $p_{calc}=E_{calc}$ being respectively the measured energy of the photon and the energy obtained from the calculation. $\chi^2_{photons}$ was used only to validate $\tau^+\tau^-\gamma\gamma$ candidates.

The errors $\sigma(p)/p$, which consisted of a convolution of the experimental errors and the uncertainty of the calculation procedure, were derived from the simulation of e$^+$e$^- \rightarrow$ Z$^0 \rightarrow \ell^+\ell^-$X, X $\rightarrow \gamma\gamma$. An error of $\sigma(p)/p = 0.05$ was estimated for charged particles associated with a signal in the muon chambers (muons), and an error of $\sigma(p)/p = 0.2$ was established for all other charged particles, which were considered a priori as possible electron candidates. These errors are larger than those found in the standard DELPHI tracking system as they reflect the photon angular errors; for the electron candidates, a large error is introduced by bremsstrahlung losses.

For $\tau^+\tau^-\gamma\gamma$ candidates, where the uncertainty on the momentum calculation is larger than the measured value, an uncertainty of $\sigma(p)/p=\sigma(E)/E = (35\%/\sqrt{E} + 9\%)$ was estimated for the photons.

Figure 2 shows the χ^2 distributions for charged particles and for photons for simulated doubly radiative events (as predicted by second order QED) and for simulated e$^+$e$^- \rightarrow$ Z$^0 \rightarrow \ell^+\ell^-$X, X $\rightarrow \gamma\gamma$ signal events. In the e$^+$e$^-\gamma\gamma$ and $\mu^+\mu^-\gamma\gamma$ channels, good agreement is observed between measured and calculated momenta ($\chi^2_{charged}\leq 5$ for most of the events), whereas in the $\tau^+\tau^-\gamma\gamma$ channel, the measured and calculated momenta differ substantially ($\chi^2_{charged}\geq 20$). As expected, the same behaviour is observed in both the QED events and the signal events. The tail extending to high $\chi^2_{charged}$ values in the $\mu^+\mu^-\gamma\gamma$ channel results from detector edge effects.

Events were selected as :

– $\mu^+\mu^-\gamma\gamma$ if $\chi^2_{charged}$ was lower than 5 and at least one of the two selected charged particles had one or more hits in the muon chambers;
– e$^+$e$^-\gamma\gamma$ if $\chi^2_{charged}$ was lower than 5, the charged particles were not previously selected as muons, and the

Table 1. Efficiencies obtained after applying the selection criteria to the simulated e$^+$e$^- \rightarrow$ Z$^0 \rightarrow \ell^+\ell^-$X, X $\rightarrow \gamma\gamma$ events

Channel	$m_{\gamma\gamma} = 60$ GeV/c^2	$m_{\gamma\gamma} = 10$ GeV/c^2
e$^+$e$^-\gamma\gamma$	37%	35%
$\mu^+\mu^-\gamma\gamma$	40%	36%
$\tau^+\tau^-\gamma\gamma$	19%	13%

Table 2. Results obtained from data taken from 1991 to 1994 for $m_{\gamma\gamma}$ above 10 GeV/c^2, together with the QED expectations

Channel	Observed	Expected
e$^+$e$^-\gamma\gamma$	31	31 ± 5
$\mu^+\mu^-\gamma\gamma$	32	31 ± 3
$\tau^+\tau^-\gamma\gamma$	16	14 ± 2
Total	79	76 ± 6

ratio between the sum of the electromagnetic energy associated to the charged particles and the sum of their momenta exceeded 0.2;
– $\tau^+\tau^-\gamma\gamma$ if $\chi^2_{charged}$ was higher than 20 and $\chi^2_{photons}$ was lower than 9.

Events with $5 < \chi^2_{photons} < 10$ were also scanned to check for possible edge effects between HPC modules. In particular, if energy was deposited in the hadronic calorimeter behind the gaps between HPC modules, this energy was associated to the measured electromagnetic energy.

The efficiencies obtained for simulated e$^+$e$^- \rightarrow$ Z$^0 \rightarrow \ell^+\ell^-$X, X $\rightarrow \gamma\gamma$ events are presented in Table 1.

A total of 79 events were found satisfying the topological and lepton identification selection and with a two photon invariant mass larger than 10 GeV/c^2 . Of these, 31 were identified as e$^+$e$^-\gamma\gamma$ candidates, 32 as $\mu^+\mu^-\gamma\gamma$ and 16 as $\tau^+\tau^-\gamma\gamma$.

3.3 Results

The distribution of $\gamma\gamma$ masses obtained, using the values calculated for the energy of the photons, is presented in Fig. 3 and compared with the second order QED predictions, obtained through Monte Carlo simulation and normalized to the total integrated luminosity collected by DELPHI from 1991 to 1994.

Table 2 compares the numbers of events obtained for masses above 10 GeV/c^2 with the numbers expected for all channels. Figure 4 shows the distribution of the lowest photon isolation angle and of the invariant mass of the two leptons for the events satisfying the selection criteria described above. There is overall agreement between the expected and observed distributions, but there is nevertheless a small excess of events in the data, relative to the simulation, in the high $\gamma\gamma$ mass region on Fig. 3. According to the QED simulation, 2.3 ± 1.2 events are expected above 50 GeV/c^2 , while 6 events (3 e$^+$e$^-\gamma\gamma$, 2 $\mu^+\mu^-\gamma\gamma$ and one $\tau^+\tau^-\gamma\gamma$) are found in the data.

For $\mu^+\mu^-\gamma\gamma$ and e$^+$e$^-\gamma\gamma$ events with $m_{\gamma\gamma} > 50$ GeV/c^2 a kinematical constraint was applied, including a test on the hypothesis of initial state radiation contained in the beam pipe, in order to evaluate the migration of events with low mass to the high mass region because of wrong angles due to an additional photon. In applying the kinematical constraint,
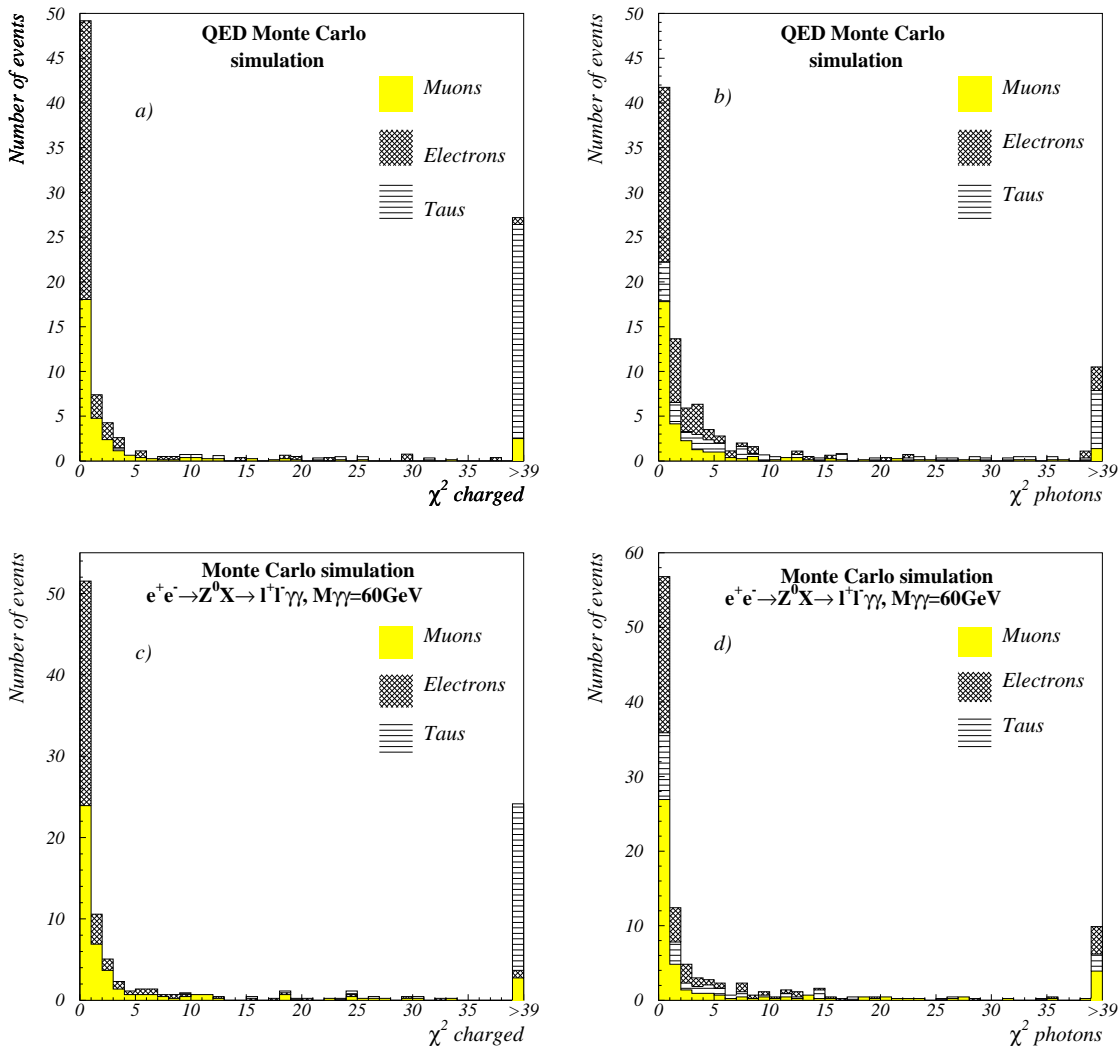
Fig. 2. $\chi^2_{charged}$ ($\chi^2_{photons}$) distribution obtained with the QED Monte Carlo simulation, **a) b)**, and with the signal simulation $e^+e^- \rightarrow Z^0 \rightarrow \ell^+\ell^-X$, $X \rightarrow \gamma\gamma$, **c) d)**. In each figure, χ^2 values higher than 39 are accumulated in the last bin

a variation of 1 standard deviation was allowed for the measured angles and the ISR energy was obtained for the best χ^2, calculated using both the angles and the momenta of the charged particles. The results are shown in Table 3. There is no significant difference between the $\gamma\gamma$ mass obtained before and after including ISR, as the ISR is not large. As an example one of the events, a $\mu^+\mu^-\gamma\gamma$ event with $m_{\gamma\gamma} = 58.0$ GeV/c^2 , is shown in Fig. 5.

No other significant accumulation of events was seen in any region of the $\gamma\gamma$ mass spectrum. The limit at 95% confidence level on BR($Z^0 \rightarrow \ell^+\ell^-X$) $\times$ BR($X \rightarrow \gamma\gamma$) (Fig. 6) was obtained for the sum of the three lepton species as a function of the two photon invariant mass. The limit was estimated using Poisson statistics including the estimate of the background. In calculating the limit, a bin width of 2 GeV/c^2 was used, which matches the mass resolution of about 1 GeV/c^2 .

4 Decays into two neutrinos and two photons

The massive X particle could also be produced with a virtual Z^0 which would decay into two neutrinos. The possible X decay into two photons would give rise to events with two energetic photons in the final state with large acoplanarity plus missing energy and momentum. Such events are easily separable from the QED background process $e^+e^- \rightarrow \gamma\gamma$ [11] through an acoplanarity cut.

Events were selected according to the following criteria:

- Two and only two clusters with an electromagnetic energy greater than 15 GeV in the HPC or FEMC ($\theta > 25°$). In addition it was required that there were no other clusters isolated from these by more than $6°$ and having an energy above 3 GeV . Events with HPC clusters aligned with TPC sector boundaries were excluded to avoid e^+e^- contamination.
- No charged particle tracks reconstructed in the TPC pointing to the main interaction point.
- Energy in the hadron calorimeter less than 5 GeV and a requirement that the HPC clusters with more than 15

Table 3. Characteristics of the selected $\ell^+\ell^-\gamma\gamma$ events with $\gamma\gamma$ masses above 50 GeV/c^2. The $\gamma\gamma$ and $\ell\ell$ masses are given both before and after considering the hypothesis of initial state radiation contained in the beam pipe

Channel	$\gamma\gamma$ mass (GeV/c^2)		$\ell\ell$ mass (GeV/c^2)		Lowest $\ell\gamma$	ISR	χ^2
	without ISR	with ISR	without ISR	with ISR	isolation angle (°)	(GeV)	
$\mu^+\mu^-\gamma\gamma$	50.3 ± 0.2	51.0 ± 0.8	34.8 ± 0.1	32.6 ± 2.0	63.5	1.80	0.8
$\mu^+\mu^-\gamma\gamma$	57.8 ± 0.1	58.0 ± 0.2	29.1 ± 0.1	27.5 ± 1.0	38.6	0.95	1.4
$e^+e^-\gamma\gamma$	58.6 ± 0.2	58.8 ± 1.0	6.6 ± 0.3	6.5 ± 0.5	15.8	0.05	9.4
$e^+e^-\gamma\gamma$	62.2 ± 0.1	62.3 ± 0.5	20.7 ± 0.1	20.8 ± 0.5	21.3	0.05	5.1
$e^+e^-\gamma\gamma$	63.8 ± 0.3	63.9 ± 1.0	13.6 ± 0.3	13.5 ± 0.6	25.4	0.05	0.6
$\tau^+\tau^-\gamma\gamma$	69.1 ± 0.5	-	18.8 ± 1.0	-	16.4	-	-
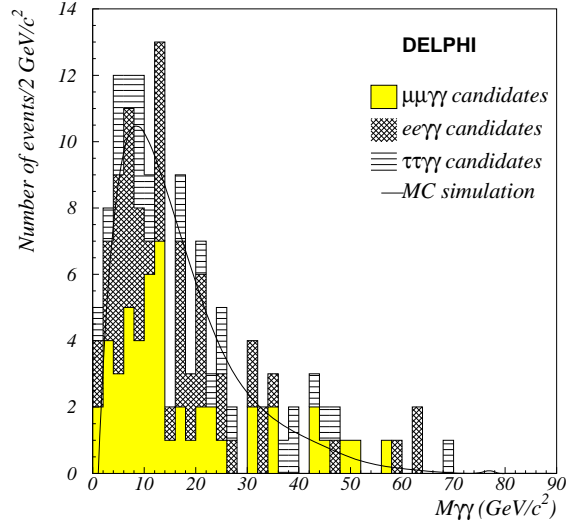
Fig. 3. Invariant mass of the two photons for the candidates selected from 1991 to 1994, together with the QED simulation expectations

GeV point to the interaction vertex within 10 degrees; these requirements rejected most cosmics.

- For HPC photons with more than 15 GeV, the most energetic HPC layer should not contain more than 50% of the total cluster energy and the number of layers with an energy deposition greater than 5% of the cluster energy should be greater than three. This cut rejects background due to radioactivity in the lead of the HPC.

The distribution of the acoplanarity angle between the two photons is shown in Fig. 7. The data distribution is slightly wider than that predicted by the Monte Carlo simulation including second order QED processes [11], but the agreement is adequate for the present purpose. No event was found with an acoplanarity greater than 10°. The efficiency for the channel $Z^0 \to \nu\bar{\nu}X$, where X is a 60 GeV/c^2 resonance decaying into two photons, was estimated as (23 ± 2)%, for a trigger efficiency of 97% computed from a Bhabha data sample and the trigger redundancy. This result can be translated into a 95% confidence level upper limit of BR($Z^0 \to \nu\bar{\nu}X$) $\times$ BR($X \to \gamma\gamma$) $< 3.7 \times 10^{-6}$.

5 Decays into a quark pair and two photons

5.1 Event selection

The analysis of $Z^0 \to q\bar{q}\gamma\gamma$ events was divided into two separate steps: first, hadronic Z^0 decays were selected, then
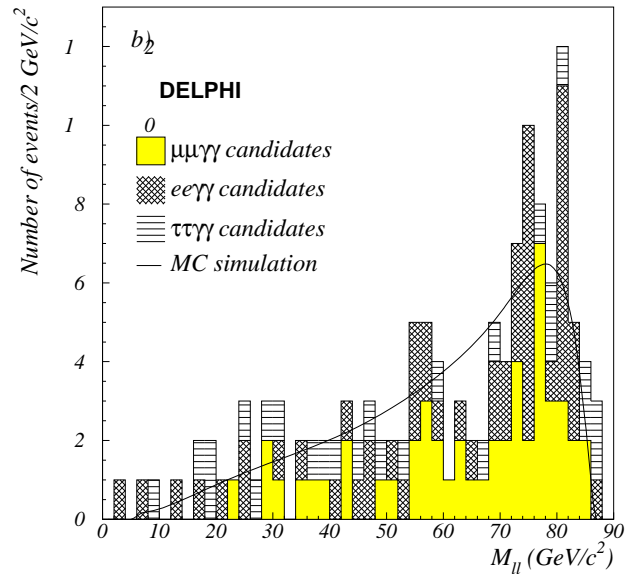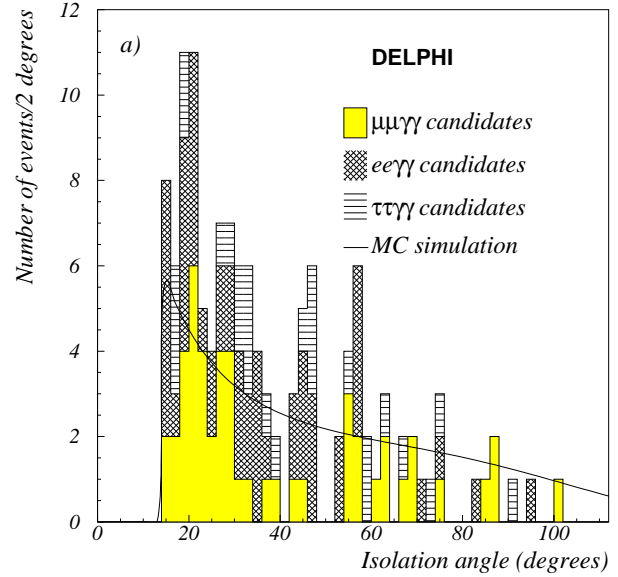

Fig. 4. a) Lowest photon isolation angle. **b)** Invariant mass of the two leptons ($m_{\ell\ell}$)

$q\bar{q}\gamma\gamma$ candidates were identified by looking for pairs of high energy isolated photons in the selected hadronic sample.

Hadronic Z^0 decays were selected on the basis of charged multiplicity (N_{ch}) and total visible energy (E_{vis}) by the conditions $N_{ch} \geq 5$ and $E_{vis} \geq 20\%\sqrt{s}$, where $\sqrt{s}$ is the centre-of-mass energy. For the computation of the charged
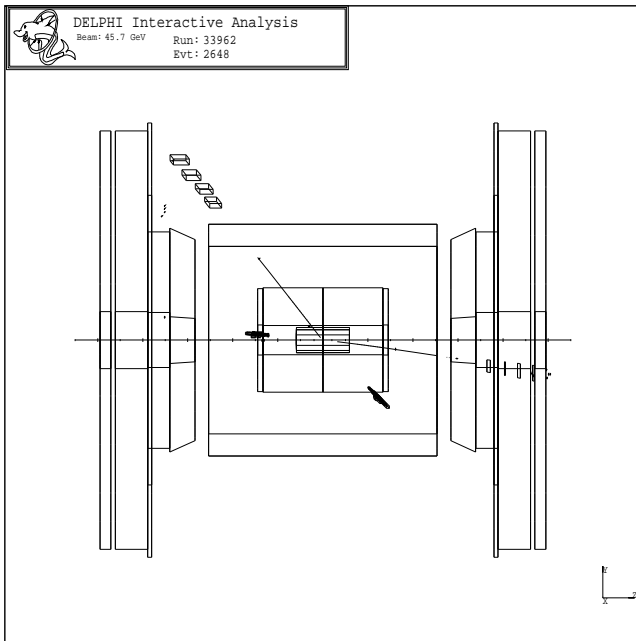
Fig. 5. Display on the yz plane of the $\mu^+\mu^-\gamma\gamma$ event with $m_{\gamma\gamma} = 58.0$ GeV/c^2 . Starting from the interaction region, the detectors shown in the figure represent the Inner Detector, Time Projection Chamber, Barrel Electromagnetic Calorimeter, Forward Electromagnetic Calorimeter and Hadron Calorimeter. The four particles in the figure have angles θ and ϕ (θ is the polar angle defined with respect to the z axis, represented in the figure, and ϕ is the angle in the plane perpendicular to z axis) of $\theta = 64.2°$, $\phi = 329.8°$ and $\theta = 120.0°, \phi = 177.0°$ for the two photons and $\theta = 125.0°$, $\phi = 115.6°$ and $\theta = 27.4°, \phi = 347.5°$ for the two muons
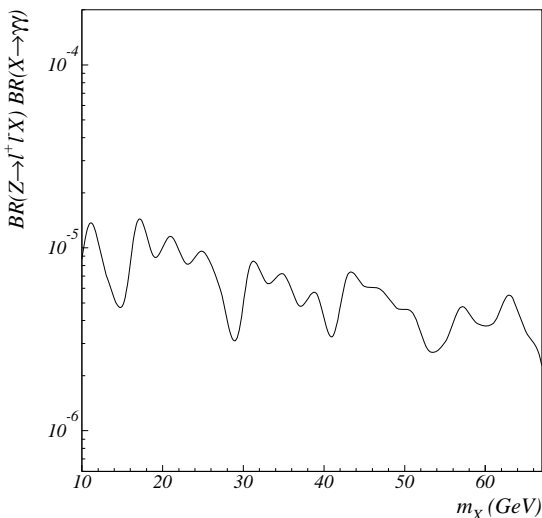
Fig. 6. Limit at 95% Confidence Level on BR($Z^0 \to \ell^+\ell^-$X) × BR(X → $\gamma\gamma$) as a function of the X particle mass

multiplicity and of the visible energy, as well as for the final physics analysis, only well reconstructed charged particles with momentum $p > 0.4$ GeV/c and neutral particles with associated energy $E > 0.5$ GeV were considered. The statistics collected with these criteria in the years 1991 to 1994 amounts to 3,253,000 Z^0 decays. The efficiency for $Z^0 \to q\bar{q}$ events is (98.4 ± 0.1)%, while the contamination from $Z^0 \to \tau^+\tau^-$ events is estimated to be (0.4 ± 0.1)%.
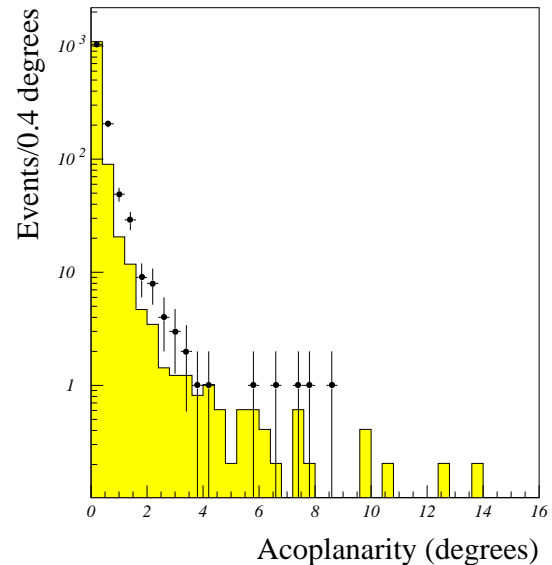
Fig. 7. Distribution of the acoplanarity angle between the two photons for data (dots) and Monte Carlo simulation (shaded area)

The identification of the events with two isolated photons relied on the presence of at least two neutral showers in the electromagnetic calorimeters each satisfying the following requirements:

– energy $E_\gamma > 3.0$ GeV,
– shower shape compatible with that expected for genuine single photons [5],
– isolation angle $\delta_\gamma > 15°$ with respect to all well reconstructed charged particles with momentum $p > 0.4$ GeV/c and neutral particles with energy $E > 0.5$ GeV, with the only exception of the other photon candidate which is allowed to violate the isolation condition.

Isolated photon candidates were accepted in the full angular range covered by HPC and FEMC, which roughly corresponds to the region $9° < \theta_\gamma < 171°$. However, only the events in which at least one photon satisfied the condition $25° < \theta_\gamma < 155°$ were considered in the analysis. Isolated photons detected in the very forward region, that is below the FEMC inner radius, were rejected to avoid a significant contamination from initial state radiation. The events in which both photons were detected at an angle smaller than $25°$ from the beam axis were rejected because the reduced tracking efficiency in the forward region could spoil the isolation criteria.

The requirement of a minimum isolation angle between each photon and the other particles is motivated by the need to reduce the main Standard Model backgrounds, which consist of secondary photons from π^0 decays, prompt electromagnetic radiation from quarks, and long lived neutral hadrons interacting in the electromagnetic calorimeters. In fact, while the background is concentrated in the hadronic jets, photons produced in the decay of a large mass resonance are expected to be well isolated.

All particles excluding the two photon candidates were clustered into two jets by means of the K_T (also known as 'Durham') algorithm [12]. In this algorithm, pairs of 'particles' are iteratively recombined into jets beginning with

the pair with the lowest value of a scaled invariant mass variable, y_{ij}, given by

$$y_{ij} = \frac{2 \min(E_i^2, E_j^2)(1 - \cos \theta_{ij})}{E_{vis}^2}, \qquad (1)$$

where E_i is the energy of 'particle' i and θ_{ij} is the angle between 'particles' i and j. The 'particles' may be individual particles or recombined 'jets'. In this analysis the procedure was applied iteratively until precisely two jets were found.

By applying a constrained fit, which relies on energy and momentum conservation as well as on the measured energies and directions of the two jets and of the two isolated photons, a better estimate of the photon energies was obtained than that provided by the electromagnetic calorimeters alone. The events in which the fitted photon energies differed from the calorimetric measurements by more than $2.5\sigma_\gamma$, where σ_γ is the calorimeter energy resolution, were rejected. If two or more photon-pairs belonging to the same event satisfied all selection criteria, only the pair with largest invariant mass was considered.

As for the leptonic channels, the efficiency in the search for a high mass resonance (X) decaying into two photons was estimated by simulating the Bjorken process $Z^0 \rightarrow Z^*X$ with the X particle decaying into photons and the Z^* into hadrons. Masses of 10, 30 and 60 GeV/c^2 were considered for the X particle. The $\gamma\gamma$ mass resolution obtained was $\sigma_m = 1.0$ GeV/c^2, $\sigma_m = 1.5$ GeV/c^2 and $\sigma_m = 2.0$ GeV/c^2 for the three masses considered. The signal efficiency was about 18%, 24% and 18% respectively. The resolution and the efficiency in the full mass range were obtained by linear extrapolation.

5.2 Results

The $\gamma\gamma$ invariant mass ($m_{\gamma\gamma}$) distribution for the events passing all selection criteria and having $m_{\gamma\gamma} < 5$ GeV/c^2 is shown in Fig. 8. The shaded area in the figure shows the (smoothed) simulation of the $Z^0 \rightarrow q\bar{q}$ and $Z^0 \rightarrow \tau^+\tau^-$ processes provided by the JETSET 7.3 PS [10] and KORALZ [13] models, respectively. JETSET 7.3 PS is based on the leading-log approximation for multiple photon and gluon radiation and on the Lund String Fragmentation Model [14] for the simulation of the hadronization process. The generated statistics amount to about six million $Z^0 \rightarrow q\bar{q}$ decays and $700,000$ $Z^0 \rightarrow \tau^+\tau^-$ decays. All generated events were also passed through a complete simulation of the DELPHI detector [5].

In the low-mass region of Fig. 8, the two peaks corresponding to the π^0 and η masses are clearly visible. As also observed in the study of prompt photons in hadronic decays [15], more isolated π^0 production is observed than predicted by JETSET 7.3 PS. In order to reproduce the data in the low $m_{\gamma\gamma}$ region better, the yield of isolated π^0 mesons (for which no other particle was reconstructed within 15° from their flight direction) was increased by a factor 1.6 in the simulation by means of a reweighting procedure. Following reference [15], the yield of isolated final state photons was also increased by 18% in the simulation. The $\gamma\gamma$ invariant mass distribution after applying the reweighting
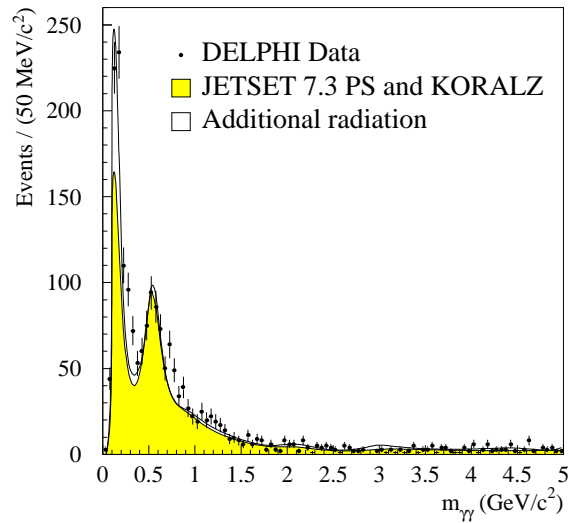

Fig. 8. The $\gamma\gamma$ invariant mass distribution of the events satisfying all selection criteria and having $m_{\gamma\gamma} < 5$ GeV/c^2. The shaded area shows the (smoothed) distribution of the background simulation based on JETSET 7.3 PS for the process $Z^0 \rightarrow q\bar{q}$, and on KORALZ for the process $Z^0 \rightarrow \tau^+\tau^-$. The region in white describes the additional radiation introduced by rescaling the isolated π^0 and final state radiation yields
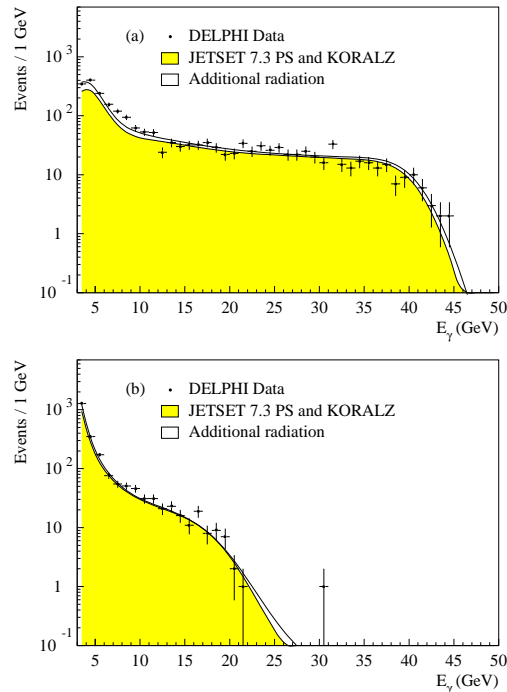

Fig. 9. The energy spectrum of the higher energy **(a)** and lower energy **(b)** photon in the selected photon pairs. The meaning of the white and shaded regions is the same as in Fig. 8

procedure is superimposed on the original JETSET 7.3 PS simulation in Fig. 8. The energy spectra of the higher and lower energy photons are plotted in Fig. 9. As shown in the figure, the additional radiation introduced by increasing the isolated π^0 yield improves the agreement between the data and the simulated background.

The $\gamma\gamma$ invariant mass distribution in the region $m_{\gamma\gamma} > 5$ GeV/c^2 region is shown in Fig. 10. In particular, in the

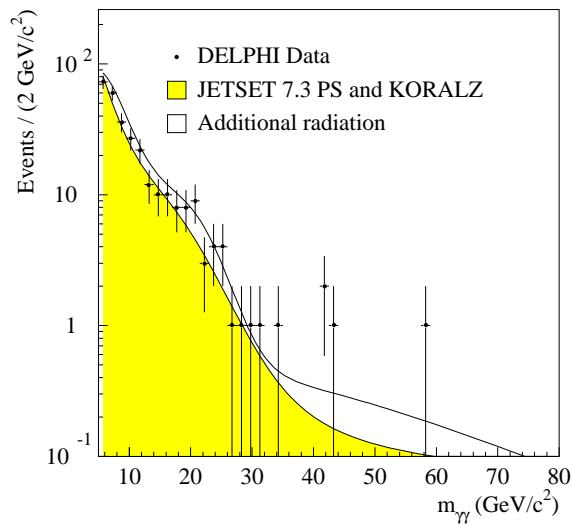**Fig. 10.** The $\gamma\gamma$ invariant mass distribution of the events satisfying all selection criteria and having $m_{\gamma\gamma} > 5$ GeV/c^2. The meaning of the white and shaded regions is the same as in Fig. 8
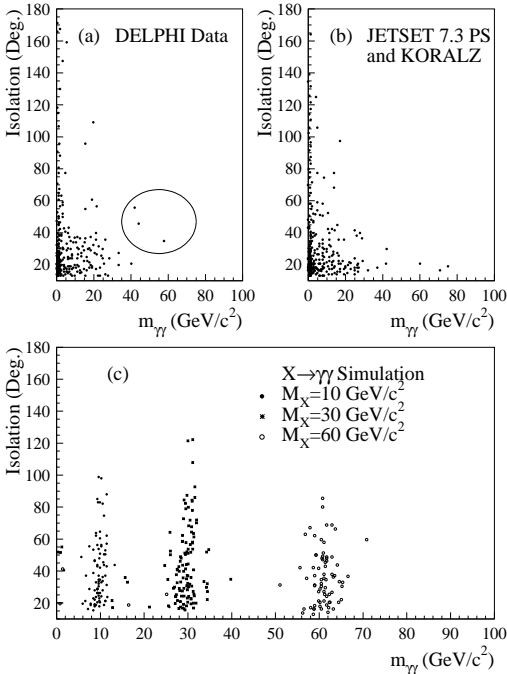

Fig. 11. Plot of the minimum isolation angle of the two photons versus their invariant mass as observed in the data **(a)**, in the background simulation **(b)** and in the signal simulation **(c)**. The ellipse in plot **(a)** surrounds the three data events having $m_{\gamma\gamma} > 30$ GeV/c^2 and unusual photon isolation. The statistics in plot **(b)** is that obtained from an initial sample of about 6 million simulated hadronic events without rescaling the π^0 yield

region $m_{\gamma\gamma} > 30$ GeV/c^2, 6 events were reconstructed in the data while 3.7 ± 1.3 and 5.6 ± 1.9 events are predicted by the original and the reweighted background simulation respectively.

The correlation between the minimum isolation angle of the two photons (that is the smaller of $\delta_{\gamma 1}$ and $\delta_{\gamma 2}$) and the $\gamma\gamma$ mass is plotted in Fig. 11 for the data, the background simulation and the simulation of signals for the three considered X particle masses. The statistics in Fig. 11 (b) is that obtained from an initial sample of about 6 million simulated
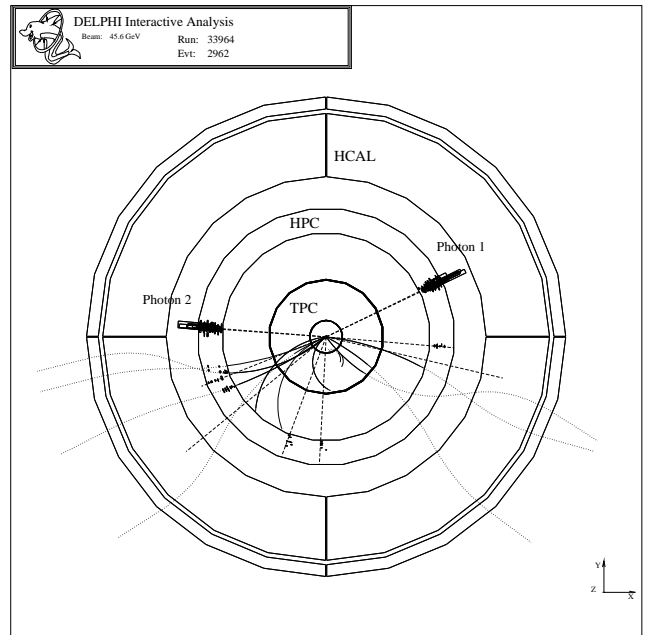

Fig. 12. Display of the $q\bar{q}\gamma\gamma$ candidate event with $m_{\gamma\gamma} = 57.9$ GeV/c^2. Starting from the interaction region, the detectors shown in the figure represent the Time Projection Chamber (TPC), the Barrel Electromagnetic Calorimeter (HPC) and the Hadron Calorimeter (HCAL)
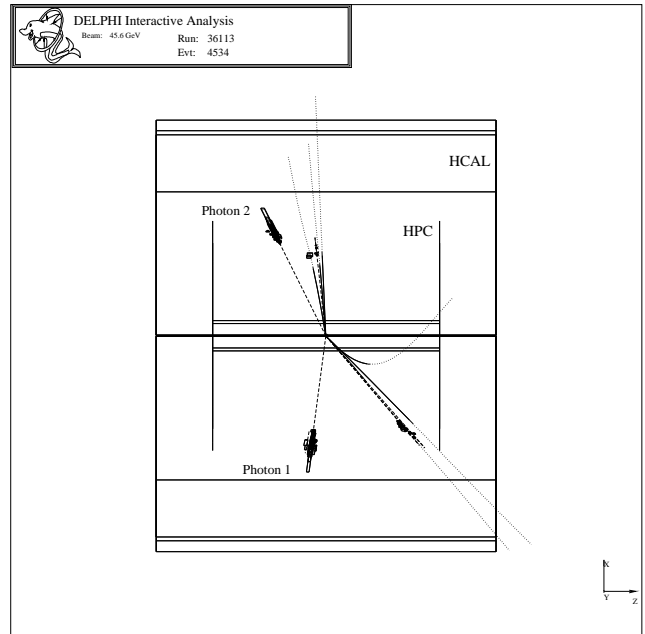

Fig. 13. Display of the $q\bar{q}\gamma\gamma$ candidate event with $m_{\gamma\gamma} = 43.6$ GeV/c^2. The figure also shows the schematic profiles of the Barrel Electromagnetic Calorimeter (HPC) and of the Hadron Calorimeter (HCAL)

hadronic events without rescaling the π^0 yield. The distribution of the data events in Fig. 11 (a) is similar to that predicted by the simulation for the $Z^0 \to q\bar{q}$ (and $Z^0 \to \tau^+\tau^-$) background. However three events in the data have photon pairs with $m_{\gamma\gamma} > 30$ GeV/c^2 and unexpectedly large isolation. These events are described in Table 4 and shown in Figs. 12 to 14.

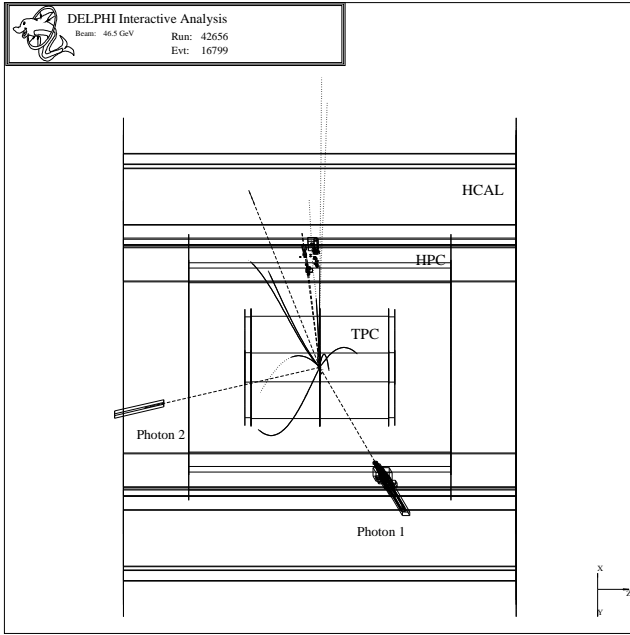**Fig. 14.** Display of the q$\bar{\text{q}}\gamma\gamma$ candidate event with $m_{\gamma\gamma} = 41.8$ GeV/c^2 . The figure also shows the lateral profiles of the Time Projection Chamber (TPC), of the Barrel Electromagnetic Calorimeter (HPC) and of the Hadron Calorimeter (HCAL)

Table 4. The characteristics of the three events observed in the data with unexpected photon isolation and large $\gamma\gamma$ mass. The estimates for the photon energy, the $\gamma\gamma$ mass and jet-jet mass are obtained from a constrained fit on the two photons and the two jets

Run/Event	33964/2962	36113/4534	42656/16799
$E_{\gamma 1}$ (GeV)	30.3	27.0	38.1
$\theta_{\gamma 1}$ ($^\circ$)	81.0	97.4	62.9
$\phi_{\gamma 1}$ ($^\circ$)	26.0	176.2	150.1
$E_{\gamma 2}$ (GeV)	30.2	19.5	16.8
$\theta_{\gamma 2}$ ($^\circ$)	118.9	115.8	160.9
$\phi_{\gamma 2}$ ($^\circ$)	175.8	12.8	72.7
$m_{\gamma\gamma}$ (GeV/c^2)	57.9± 1.7	43.6± 1.8	41.8± 1.1
$m_{jet-jet}$ (GeV/c^2)	24.7± 2.6	41.7± 2.4	14.1± 2.6

As no relevant accumulation is visible in the $\gamma\gamma$ mass distribution, no evidence for Z^0 → q$\bar{\text{q}}$X(X → $\gamma\gamma$) decays can be inferred from the data. Therefore a limit on BR(Z^0 → q$\bar{\text{q}}$X)×BR(X → $\gamma\gamma$) can be set as a function of the X particle mass. The limit at 95% confidence level, as obtained after rescaling the isolated π^0 yield in the background simulation, is plotted in Fig. 15.

6 Conclusions

Events with high mass photon pairs from the processes e$^+$e$^-$ → $\ell^+\ell^-\gamma\gamma$, e$^+$e$^-$ → $\nu\bar{\nu}\gamma\gamma$ and e$^+$e$^-$ → q$\bar{\text{q}}\gamma\gamma$ have been sought in a data sample containing 3.5 million hadronic Z^0 's, collected with the DELPHI detector at LEP during the years 1991 to 1994.

In the $\ell^+\ell^-\gamma\gamma$ channel, 79 events with two charged leptons and two isolated photons were selected with photon pair masses above 10 GeV/c^2 , where 76 ± 6 events were predicted from standard sources. A slight excess of events in the data compared to the predictions from QED processes
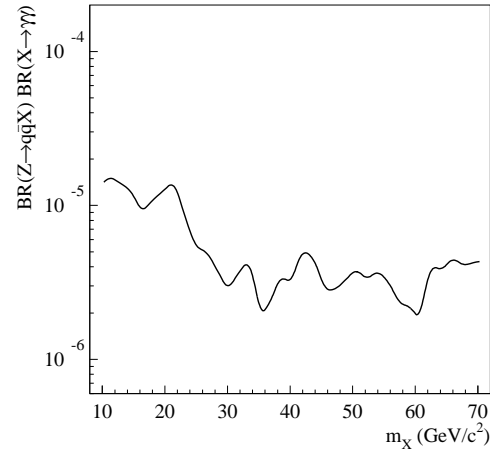

Fig. 15. The limit at 95% confidence level on BR(Z^0 → q$\bar{\text{q}}$X)×BR(X → $\gamma\gamma$) as a function of the X particle mass

was found for $\gamma\gamma$ mass regions above 50 GeV/c^2 , where 6 events were observed while 2.3 ± 1.2 events were predicted from standard sources.

No $\nu\bar{\nu}\gamma\gamma$ candidates were found with an acoplanarity between the two photons exceeding 10°.

In the hadronic channel, the $\gamma\gamma$ invariant mass distribution in the region $m_{\gamma\gamma} > 10$ GeV/c^2 was found to be compatible with that expected from the simulation of the standard Z→ q$\bar{\text{q}}$ process after rescaling the isolated π^0 yield as indicated by the data in the low $m_{\gamma\gamma}$ region. However three large-mass q$\bar{\text{q}}\gamma\gamma$ events with unusual photon isolation were observed in the data.

No evidence was found for events clustering in $\gamma\gamma$ mass regions above 10 GeV/c^2 in any channel considered. The limits obtained on the Z^0 branching ratios, for invariant masses of the two photons above 30 GeV/c^2 are of the order of 3 to 4×10^{-6}. These results can be translated directly into a limit on the branching ratio BR(Z^0 → Z*X) × BR(X → $\gamma\gamma$) of the same order of magnitude.

References

1. L3 Collaboration, O. Adriani et al., Phys. Lett. **B295** (1992) 337.
2. OPAL collaboration, P.D.Acton et al., Phys. Lett. **B311** (1993) 391.
3. ALEPH collaboration, D. Buskulic et al., Phys. Lett. **B308** (1993) 425.
4. V. Barger et al., "A Separate Higgs?", **ANL-HEP-PR-92-102 MAD/PH/728 OITS-499** (1992), hep-ph/9211234;
   M. A. Díaz and T. J. Weiler, "Decays of a fermiophobic Higgs", **VAND-TH-94-1** (1994), hep-ph/9401259;
   S. Barshay and P. Heiliger, Mod. Phys. Lett. **A9** (1994) 11;
   K. Akama and H. Terazawa, Phys. Lett. **B321** (1994) 145.
5. DELPHI Collaboration, P. Abreu et al., Nucl. Instr. and Meth. **A378** (1996) 57.
6. W.J. Stirling, Phys. Lett. **B271** (1991) 261.
7. S. Jadach and B.F.L. Ward, Phys. Lett. **B247** (1992) 470.
8. D.J. Summers, Phys. Lett. **B302** (1993) 326.
9. M. Martinez and R. Miquel, Phys. Lett. **B302** (1993) 108.

10. T. Sjöstrand, Comp. Phys. Comm. **39** (1986) 347;
    T. Sjöstrand, Pythia 5.6 and JETSET 7.3, **CERN-TH/6488-92.**
11. F.A.Berends, R.Kleiss, Nucl. Phys. **B186** (1981) 22.
12. S. Catani et al., Nucl. Phys. **B407** (1993) 3.

13. S. Jadach and Z. Was, Comp. Phys. Com. **36** (1985) 191;
    S. Jadach, B.F.L. Ward and Z. Was, Comp. Phys. Com. **66** (1991) 276.
14. B. Andersson et al., Phys. Rep. **97** (1983) 31.
15. DELPHI Collaboration, P. Abreu et al., Zeit. Phys. **C69** (1995) 1.